Prepared for submission to JHEP

ZU-TH 18/14
MCnet-14-09
LPN14-068
IPPP/14/34
DCPT/14/68

arXiv:1404.7139v2 [hep-ph] 13 Aug 2014

Standard Model Higgs boson pair production in the $(b\bar{b})(b\bar{b})$ final state

Danilo Enoque Ferreira de Lima,[1,3] **Andreas Papaefstathiou,**[2] **Michael Spannowsky**[3]

[1] *University of Glasgow, United Kingdom*
[2] *Institut für Theoretische Physik, Universität Zürich, Switzerland*
[3] *Institute for Particle Physics Phenomenology, Durham University, United Kingdom*

E-mail: dferreir@mail.cern.ch, andreasp@physik.uzh.ch, michael.spannowsky@durham.ac.uk

Abstract: Measuring the Higgs boson couplings as precisely as possible is one of the major goals of the High Luminosity LHC. We show that the $(b\bar{b})(b\bar{b})$ final state in Higgs boson pair production can be exploited in the boosted regime to give constraints on the trilinear Higgs boson self-coupling. In these exclusive phase space regions, novel jet substructure techniques can be used to separate the signal from the large QCD and electroweak backgrounds. New developments on trigger and b-tagging strategies for the upcoming LHC runs are necessary in order to reconstruct the Higgs bosons in boosted final states, where the trilinear self-coupling sensitivity is reduced. We find that using our approach one can set a limit for $\lambda \leq 1.2$ at 95% CL after 3000 fb^{-1}. As the signal-to-background ratio is small, we propose a data-driven side-band analysis to improve on the coupling measurement.

Contents

1 Introduction **1**

2 Phenomenological considerations **3**
- 2.1 Kinematics 3
- 2.2 Event selection and triggering 4
- 2.3 Reconstruction techniques 6

3 Simulation and analysis **7**
- 3.1 Signal and backgrounds 7
- 3.2 Basic analysis 8
- 3.3 Constraints 11
- 3.4 Side band analysis 13

4 Conclusions **14**

1 Introduction

The Standard Model (SM) provides an exceptionally good description of the observed phenomena in the realm of elementary particles, with very few exceptions, linked to much higher energy scales that for the time being may lie beyond experimental reach.[1] The epitomization of this success has been the discovery of the final missing piece of the SM, the Higgs boson, by the CERN Large Hadron Collider (LHC) experimental collaborations during the first run at pp centre-of-mass energies of 7 and 8 TeV [1–5]. The LHC's 'Run II' is expected to start at 13 TeV and potentially reach the nominal pp energy of 14 TeV later on. Barring the exciting event of a phenomenal discovery of new physics effects, the most important next step is to directly probe and constrain the couplings of the Higgs boson to the content of the SM. Of particular interest are the couplings of the Higgs boson to itself, which will allow for understanding of the structure of the symmetry breaking potential:

$$\mathcal{V} = \frac{1}{2}M_h^2 h^2 + \lambda v h^3 + \frac{\tilde{\lambda}}{4}h^4 \,, \tag{1.1}$$

where h is the Higgs boson field, M_h is the Higgs boson mass, v is the vacuum expectation value, λ and $\tilde{\lambda}$ are the Higgs boson triple and quartic self-couplings respectively.

The Higgs mass has already been determined to a good precision in the first LHC run ($M_h \simeq 125$ GeV) and the vacuum expectation value, $v \simeq 246$ GeV, has been obtained by measurements of four-fermion interactions at low energies. These lead to the

[1] Examples of these may be the origin of neutrino masses or Grand Unification.

Standard Model predictions: $\lambda = \tilde{\lambda} = M_h^2/2v^2 \simeq 0.13$.[2] However, new physics can alter this direct correspondence and therefore, model-independently, the self-couplings λ and $\tilde{\lambda}$ can be probed only by direct measurements of multiple Higgs boson final states. The quartic coupling, $\tilde{\lambda}$ has been shown to be difficult, if not impossible, to measure, even at future colliders [8, 9]. On the other hand, over the past 20 years, several studies have shown that the prospects for the Higgs boson pair production, whose LHC cross section is a quadratic function of the triple self-coupling λ, remain uncertain and challenging both at future electron-positron collider (e.g. [10]) and at the LHC [7, 11–42].

Recent studies have demonstrated that using jet substructure techniques [43] in the boosted regime can potentially provide a reasonable constrain at the end of a high-luminosity run of the LHC [7, 17–32], tackling the final states $hh \to (b\bar{b})(\gamma\gamma)$, $hh \to (b\bar{b})(\tau^+\tau^-)$ and $hh \to (b\bar{b})(W^+W^-)$. The final state with the largest branching ratio, $hh \to (b\bar{b})(b\bar{b})$ has also been considered in passing, and was deemed to be extremely challenging [17, 44], particularly if $\lambda \approx \lambda_{\rm SM}$. The difficulties can be attributed to the enormous QCD background originating from multi-jet production, of which the irreducible channel $b\bar{b}b\bar{b}$ is also large, as well as the fact that the final state is fully hadronic and thus challenging to trigger on.[3]

As the search for the Higgs boson itself has shown, in the face of limited statistics one can rely on the combination of multiple channels to obtain the best constraints. This will always be the case in Higgs boson pair production, as the total cross section for the SM value of the triple coupling is estimated to be only $\sim 30 - 40$ fb when higher-order QCD corrections are included [7, 12, 24, 25, 51–54]. Taking the results of Ref. [22] at face value, one would get the constraints shown in Table 1 from each of the channels determined so far to be viable, given that the self-coupling has the SM value, for an integrated LHC luminosity of 3000 fb^{-1} at 14 TeV.[4] We emphasise the fact that constraints of this type are essentially self-consistency tests of the SM: deviations from $\lambda = \lambda_{\rm SM}$ would merely *indicate* the presence of new effects.

On the other hand, in Ref. [27], the magnitudes of deviations from the SM value of the self-coupling in several explicit models of new physics were estimated, given that no other dynamics associated with electroweak symmetry breaking are seen. The conclusion was that, ideally, one would like to detect deviations from $\lambda = \lambda_{\rm SM}$ that are $\mathcal{O}(20\%)$ or less. To accomplish that level of accuracy, one can for example supplement the current state of affairs with one or two channels which can constrain the self-coupling at least equally as well as the $hh \to (b\bar{b})(\tau^+\tau^-)$ or $hh \to (b\bar{b})(W^+W^-)$ channels at 3000 fb^{-1}. This argumentation illuminates the importance of opening up new search channels to the determination of the Higgs boson self-coupling.

In the present article we demonstrate the possibility of using the $pp \to hh \to (b\bar{b})(b\bar{b})$ channel at the LHC running at 14 TeV centre-of-mass energy, to constrain the self-coupling by employing jet substructure techniques [43], i.e. the so-called BDRS method [55] and

[2] Radiative corrections decrease these values by $\sim 10\%$ [6, 7].

[3] Apart from measuring the Higgs boson self-coupling, in scenarios beyond the Standard Model, the di-Higgs final state can be significantly enhanced and the decay into $(b\bar{b})(b\bar{b})$ can become a promising discovery channel [29, 30, 45–50].

[4] Note that due to the increase in cross section as λ decreases, the lower bound is more stringent.

process	constraint ($\times\lambda_{\rm SM}$)
$hh \to (b\bar{b})(\tau^+\tau^-)$	$\lambda = 1.00^{+0.40}_{-0.31}$
$hh \to (b\bar{b})(\gamma\gamma)$	$\lambda = 1.00^{+0.87}_{-0.52}$
$hh \to (b\bar{b})(W^+W^-)$	$\lambda = 1.00^{+0.46}_{-0.35}$
combination	$\lambda = 1.00^{+0.35}_{-0.23}$

Table 1: The expected constraints for an integrated LHC luminosity of 3000 fb^{-1} (14 TeV), for each of the 'viable' channels for Higgs boson pair production obtained by conservative estimates, according to Ref. [22]. The assumption used in obtaining these constraints is that the the self-coupling has the SM value. The final line provides the result originating from the naive combination in quadrature of these channels.

Shower Deconstruction [56–58]. While a variation of the former has already been used in this context in [17], here we perform a more detailed study complementing and combining the reconstruction using Shower Deconstruction.

The article is organised as follows: in Section 2 we describe some features of the kinematics of the Higgs boson pair production process and provide more detail on the reconstruction methods used. In Section 3 we provide details of the Monte Carlo simulation for the signal and background and the analysis strategy. In the same section we provide our results. Concluding remarks are given in Section 4.

2 Phenomenological considerations

2.1 Kinematics

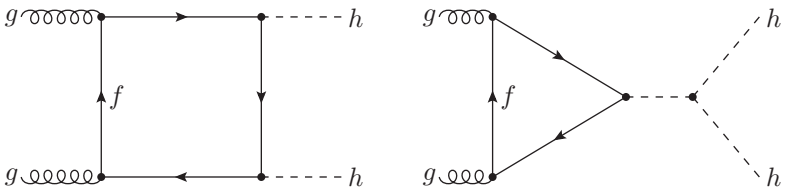

Figure 1: Higgs boson pair production diagrams contributing to the gluon fusion process at LO are shown for a fermion f. These are generic diagrams and therefore, do not include all permutations.

Higgs boson pair production at the LHC at leading order (LO) is loop-initiated and dominated by gluon fusion initial states. The contributing gluon fusion diagrams are shown in Fig. 1. We call the diagram on the left the 'box' diagram and the diagram on the right the 'triangle' diagram. The two diagrams have spin-0 configurations of the initial state gluons that interfere destructively. The box diagram also has a spin-2 configuration of

the incoming gluons. The hh cross section is a quadratic function of λ at LO, and hence possesses a minimum with respect to it. This can be shown to lie around $\lambda \sim (2.4-2.5)\lambda_{\rm SM}$, depending on the parton density functions (PDFs) employed [22]. We will only examine values on one side of the this minimum. It is natural to choose the lower half, as it includes the SM value. For completeness, we also include negative values of the self-coupling, and focus on the region $\lambda \in \{-1.0, 2.4\} \times \lambda_{\rm SM}$.

It is interesting to examine the effect of varying the self-coupling away from the SM value, on one of the characteristic distributions of the process, namely, the Higgs boson transverse momentum. In Fig. 2 we show the transverse momentum of the full process, that is, including the box and triangle diagrams as well as their interference, for several values of the self-coupling, given as multiples of the SM value. Evidently, as λ decreases the distribution of the Higgs boson transverse momentum becomes softer. This will result in a corresponding reduction of efficiency when a cut is applied on the transverse momentum of the reconstructed Higgs boson. The dip structure observed in Fig. 2, prominent for $\lambda = 2\lambda_{SM}$, is a consequence of the destructive interference between the box and triangle contributions.

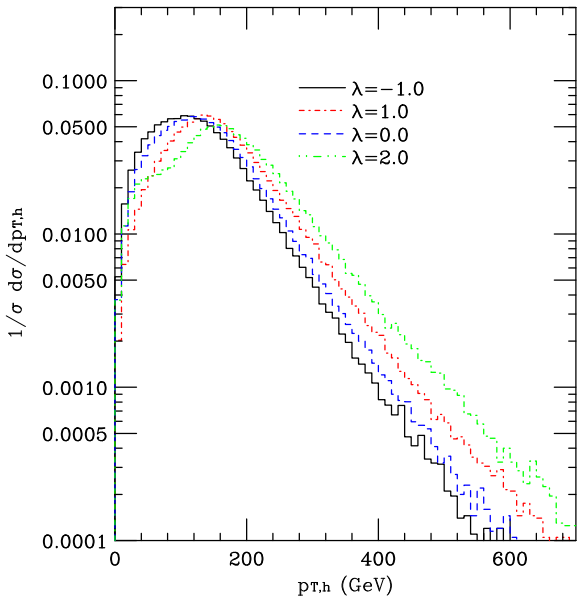

Figure 2: The transverse momentum of a Higgs boson in the pair production process, including the box and triangle diagrams as well as their interference, for several values of the self-coupling, given as multiples of the SM value.

2.2 Event selection and triggering

Triggering on events that contain purely hadronic final states is challenging.[5] This is particularly so if the masses of the resonances involved are at the electroweak scale and

[5]We do not treat b-hadrons decaying into leptons in a separate way.

their decay products have transverse momentum of only $\mathcal{O}(50)$ GeV. For the process $pp \to hh \to (b\bar{b})(b\bar{b})$ that we are considering in the present article, we have to rely on single-, di- or four-jet triggers.

Four-jet triggers designed for the upcoming LHC runs are only fully efficient for anti-k_T $R = 0.4$ jets with transverse momenta of at least 60 GeV [59]. The left panel of Fig. 3 shows the transverse momentum of the four leading b-jets in $pp \to hh \to (b\bar{b})(b\bar{b})$ at an LHC running at 14 TeV, constructed using the anti-k_t algorithm with radius parameter $R = 0.4$, before any cuts are applied. Less than 10% of the events have a fourth leading b-jet with $p_T \geq 60$ GeV. In some of those events a non-b-jet, e.g. a light hard jet produced by initial state radiation, can help satisfy the trigger requirements. However, it is evident that a large fraction of the signal is lost only due to multi-jet trigger requirements. Furthermore, using a radius parameter of $R = 0.4$ would not allow to use jet substructure techniques to reconstruct boosted Higgs bosons efficiently.

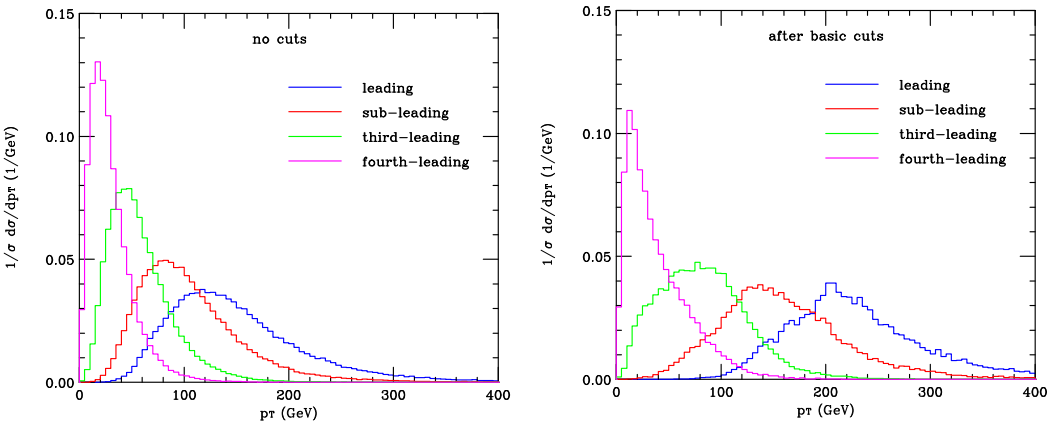

Figure 3: The transverse momentum of the four leading anti-k_t $R = 0.4$ b-jets in the SM $hh \to (b\bar{b})(b\bar{b})$ signal, before any cuts (left) and after the basic cuts as described in Section 3.2 (right).

Given that the Higgs bosons in the Standard Model $pp \to hh$ process are often boosted transverse to the beam axis (see Fig. 2) it seems to be more promising to rely on a single-jet trigger with high transverse momentum [59]. Thus, our basic event selection requires to have two jets with a large radius parameter $R = 1.2$, constructed with the Cambridge/Aachen jet algorithm. Each of these jets is required to have a transverse momentum of $p_{T,j} \geq 200$ GeV. In this regime, the main backgrounds can be substantially suppressed using jet substructure techniques, as discussed in the following section. The Higgs boson decay products should result in two b-jets contained within the large-R jet. Unfortunately, despite the fact that the large-R jet is fairly hard, the b-jets themselves can still possess a very low transverse momentum: by examining the right panel of Fig. 3, one notices that there remains a significant fraction of signal in which the fourth b-jet has a low p_T, with a substantial amount of events in the $p_T \sim 20$ GeV region, even after the $p_{T,j} \geq 200$ GeV jets are selected.

In developing the analysis of the present article, it was found that when reconstruct-

ing the Higgs bosons of the process, one must require four b-tagged subjets to facilitate background rejection. At present, good b-tagging performance with small systematic uncertainties requires a jet transverse momentum of 30-40 GeV [60]. Aiming to evaluate what the sensitivity in this channel is with existing techniques we conservatively require the b-tagged subjets inside the fat jet to have $p_{T,b} > 40$ GeV. This results in a loss of signal events and seriously limits the effectiveness of novel subjet reconstruction techniques. In this analysis, four b-tagged jets are required in each event, assuming a 70% b-tagging efficiency and a 1% light jets false identification probability.

We stress that the angular jet resolution and transverse momentum requirements for the multi-jet triggers, as well as the high momentum cut-off for b-tagging of jets and subjets severely reduce the sensitivity in this channel. Thus, an improved triggering strategy would allow for much lower p_T thresholds for the 4-jet system and a smaller R value for the jets in a real detector environment. A low-p_T jet trigger with two or three b-jets in opposite hemispheres could help to regain sensitivity in this channel for the upcoming LHC runs.

2.3 Reconstruction techniques

To reconstruct the Higgs bosons in the $(b\bar{b})(b\bar{b})$ final state we use the well established BDRS method [55] and Shower Deconstruction [56–58].[6] Both methods aim to distinguish a jet that contains the decay of products of a hadronically-decaying resonance from a jet produced by ordinary QCD processes. The jet in question is constructed with a standard jet algorithm, such as Cambridge/Aachen, using a large radius parameter $R = 1.2$ so as to capture the decay products of the heavy resonance. This is what is referred to as the 'fat jet'.

For the method Shower Deconstruction the contents of the fat jet are then used to construct narrower jets, which are called 'microjets'. Since the computational time needed to analyse an event increases fast with the number of microjets, the number is restricted by keeping the $N_{\max}$ microjets that have the highest transverse momenta, and rejecting microjets with $p_T^{\text{micro}} < p_{T,\min}^{\text{micro}}$. In what follows, we will employ $N_{\max} = 9$ and $p_{T,\min}^{\text{micro}} = 5$ GeV. The four-momenta of the microjets $\{p\}_N = \{p_1, p_2, ..., p_N\}$ are used to construct a function $\chi(\{p\}_N)$, with the property that large χ corresponds to a high likelihood that the jet has originated from the hadronic decay of a heavy resonance. Explicitly, χ is defined as

$$\chi(\{p\}_N) = \frac{P(\{p\}_N|S)}{P(\{p\}_N|B)} \,, \tag{2.1}$$

where $P(\{p\}_N|X)$ is the probability that the configuration $\{p\}_N$ is obtained, given that the event originated from sample X, where $X = S$, the signal, or $X = B$, the background. The probabilities defined above are calculated by using a simplified approximation to how a Monte Carlo event generator constructs the parton shower, as well as the decay of resonances. There are many possible histories that could lead to a given configuration, and thus one sums over the corresponding probabilities over all of them. A full description of the approximations employed and further details on the method can be found in Refs. [56, 57].

[6] Other reconstruction techniques could perform similarly [61–65].

3 Simulation and analysis

3.1 Signal and backgrounds

The signal process $pp \to hh \to (b\bar{b})(b\bar{b})$ was generated using the `Herwig++` implementation of Higgs boson pair production at LO [66–68], using the cteq6l LO PDF set. We varied the self-coupling in multiples of the Standard Model value in the region $\lambda \in \{-1.0, 2.4\} \times \lambda_{\rm SM}$ in steps of $\Delta\lambda = 0.1 \times \lambda_{SM}$. The cross section at each point was calculated at next-to-leading order (NLO) in QCD, using the `HPAIR` code [12, 14, 69] and the CT10nlo PDF sets. The black curve in Fig. 4 shows the variation of the total cross section against the Higgs boson self-coupling, λ.[7]

The irreducible QCD $b\bar{b}b\bar{b}$ background was generated using `AlpGen` [70], and passed to the `Herwig++` parton shower. The LO pdf set cteq6l was again used. The renormalization/factorization scale for the calculation was set to the sum of the squared transverse masses of the b-quarks, i.e. $\mu^2 = 4m_b^2 + \sum_i p_{Ti}^2$, where p_{Ti} are the b-quark momenta and $m_b = 4.7$ GeV. We applied the parton-level generation cuts: $p_{Tb,\rm min} = 35$ GeV, $\Delta R_{\rm min} = 0.1$, $\eta_{b,\rm max} = 2.6$, resulting in a total tree-level cross section of $\sigma_{\rm tree}(b\bar{b}b\bar{b}) \simeq 100$ pb. Using `MadGraph/aMC@NLO` [71–73], with equivalent cuts and renormalization/factorization scale and the cteq6m NLO pdf set, the NLO K-factor was estimated to be ~ 1.5. Therefore, we apply a K-factor of 1.5, resulting in a cross section $\sigma_{\rm NLO}(b\bar{b}b\bar{b}) \simeq 150$ pb.[8]

Further irreducible backgrounds arise from production of a Z boson in association with a b-quark pair, $Zb\bar{b}$, and from associated Higgs-Z boson production, hZ, with both the Z and h decaying to $b\bar{b}$. For completeness, we also consider the reducible background coming from associated production of a Higgs boson with a W boson which subsequently decays to a charm and bottom quark.[9] The $Zb\bar{b}$ background was generated using `MadGraph/aMC@NLO` at NLO in QCD, with $p_{Tb,\rm min} = 30$ GeV on the associated b-quarks. The hZ and hW backgrounds were likewise generated at NLO using `MadGraph/aMC@NLO`. The decays of Z and h to $b\bar{b}$ were generated using `Herwig++`, without any restriction imposed on the momentum of the b-quarks. Similarly, the decay of a W to a charm and a bottom quark was performed using `Herwig++`. Including the branching ratios, the NLO cross sections for these processes were found to be $\sigma_{\rm NLO}(Zb\bar{b}) \simeq 8.8$ pb, $\sigma_{\rm NLO}(hZ) \simeq 70$ fb and $\sigma_{\rm NLO}(hW) \simeq 96$ fb.

There are several additional QCD processes that may contribute as reducible backgrounds due to mis-identification of light jets or c-quark-initiated jets as b-jets. The most significant of these are QCD $b\bar{b}c\bar{c}$, $b\bar{b}jj$, $c\bar{c}c\bar{c}$, $c\bar{c}jj$ and multi-light-jet production. If we assume light-jet-to-b and c-to-b mis-tagging probabilities of 1% and 10% respectively, the total tree-level cross section contribution for the sum of these processes was estimated using `AlpGen` to be ~ 10 pb. In terms of the kinematics of the jets, these are expected to behave similarly to the reducible QCD $b\bar{b}b\bar{b}$ that we consider in the present article in detail. Hence, even considering a large K-factor of $\mathcal{O}(2)$, these processes would contribute to in-

[7] Note that the branching ratio for $hh \to (b\bar{b})(b\bar{b})$, $\simeq 0.333$, has *not* been applied to this curve.

[8] See also [74, 75] for details on NLO $b\bar{b}b\bar{b}$ production.

[9] Note however that we do not simulate charm-jet to bottom-jet mis-tagging in our analysis. Inclusion of this effect will not alter the conclusions of our analysis, since the hW background is negligible.

sample	σ_{initial} (fb)	σ_{basic} (fb)
hh, $h \to b\bar{b}$ (SM)	10.7	2.5
QCD $(b\bar{b})(b\bar{b})$	151.1×10^3	7.2×10^3
$Zb\bar{b}$, $Z \to b\bar{b}$	8.8×10^3	284.2
hZ, $h \to b\bar{b}$, $Z \to b\bar{b}$	70.0	4.1
hW, $h \to b\bar{b}$, $W \to c\bar{b}(\bar{c}b)$	96.4	5.3

Table 2: The initial cross sections for the samples considered, as well as the resulting cross sections after cuts as described by the 'basic' analysis. A K-factor of 1.5 was applied to the QCD $(b\bar{b})(b\bar{b})$ background.

crease the total QCD background cross section by $\mathcal{O}(20\%)$. For the purposes of the present phenomenological study, we do not add this contribution to the QCD background.

The second column in Table 2 demonstrates the initial cross sections, σ_{initial}, for the backgrounds considered, taking into account, where relevant, the branching ratios, the generation-level cuts and the applied K-factors.

3.2 Basic analysis

The basic analysis consists of the following simple cuts:

- lepton isolation veto: Ask for *no* isolated leptons with $p_T > 10$ GeV in the event. An isolated lepton is defined as having $\sum_i p_{T,i}$ less than 10% of its transverse momentum around a cone of $\Delta R = 0.3$ around it.
- fat jets: ask for two fat jets built via the Cambridge/Aachen algorithm with parameter $R = 1.2$ and asking for $p_T > 200$ GeV.

The resulting cross section as a function of λ, obtained after application of the basic analysis cuts to the signal samples is shown in the blue dashed curve in Fig. 4. The signal efficiency decreases with λ and hence the variation of the cross section in the region considered, after application of the basic analysis cuts is somewhat milder than that of the total NLO cross section: $\sigma^{\text{cuts}}_{\text{NLO}} \sim 1.3-5.6$ fb versus $\sigma_{\text{NLO}} \sim 15-120$ fb. The effect of the 'basic analysis' on the cross sections of all samples we have considered appear in the third column of Table 2.

The basic cuts guarantee that the effect of the lepton veto is taken into account in this analysis, which should minimise the effect of other backgrounds with an isolated lepton in the final state. It also guarantees that the hh signal has a significantly high transverse momentum, which already reduces a significant fraction of the QCD $b\bar{b}b\bar{b}$ background. Nevertheless, the impact of the backgrounds is still very large, as it can be seen in third column of Table 2, and further signal-specific constrains are necessary.

Figure 5 shows the the distribution of the difference between the rapidity values of the two large-R jets, $\Delta Y(\text{jet 1, jet 2})$, for various samples. All of the distributions peak at

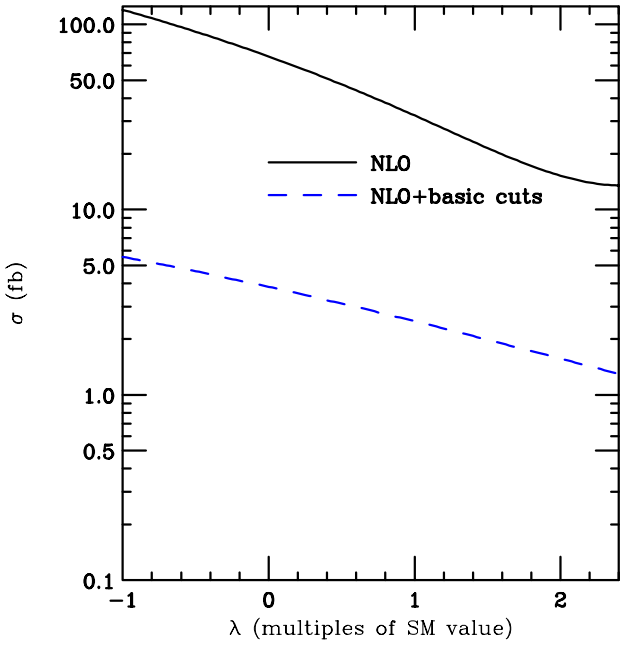

Figure 4: The black curve shows the total NLO cross section at a 14 TeV LHC calculated for each value of λ using the `HPAIR` program, not including the branching ratio for $hh \to (b\bar{b})(b\bar{b})$. The blue dashed curve shows the resulting cross section after the 'basic' analysis is applied to each signal sample, including the branching ratio for the hh decays.

$\Delta Y(\text{jet 1, jet 2}) = 0$, but evidently the hh signal has a narrower distribution compared to the dominant $Zb\bar{b}$ and QCD $b\bar{b}b\bar{b}$ backgrounds. A selection that takes only events with $\Delta Y(\text{jet 1, jet 2}) < 2.0$ can therefore be beneficial to increase background rejection.

Separating the $h \to b\bar{b}$ decay from the backgrounds can be done using substructure techniques, either through Shower Deconstruction or the BDRS reconstruction applied to the large-R jet. The Shower Deconstruction [56, 57] Higgs boson tagger has been explored as a way of discriminating the signal against the QCD multi-jet production, as described in Section 2.3. The fat jet constituents are used to calculate Cambridge/Aachen $R = 0.2$ small-R jets (i.e. the microjets) which are used as inputs for the algorithm. The leading three microjets are examined and the ones with a transverse momentum of at least 40 GeV are required to pass b-tagging criteria with a flat efficiency of 70% and a false identification rate of 1%. The Shower Deconstruction has been configured with a Higgs mass window of ± 20 GeV. The large p_T cut for the b-tagged subjets severely limits the performance of Shower Deconstruction as the invariant mass of the two b-tagged subjets is often $\sim m_H$ leaving not much phase space for wide-angle emissions off the bottom quarks. Thus, the full flexibility of this algorithm is not exploited in this analysis.

Another approach uses the BDRS [55] method to reconstruct the Higgs boson four-momentum. When using the BDRS, a mass window can be applied to the reconstructed

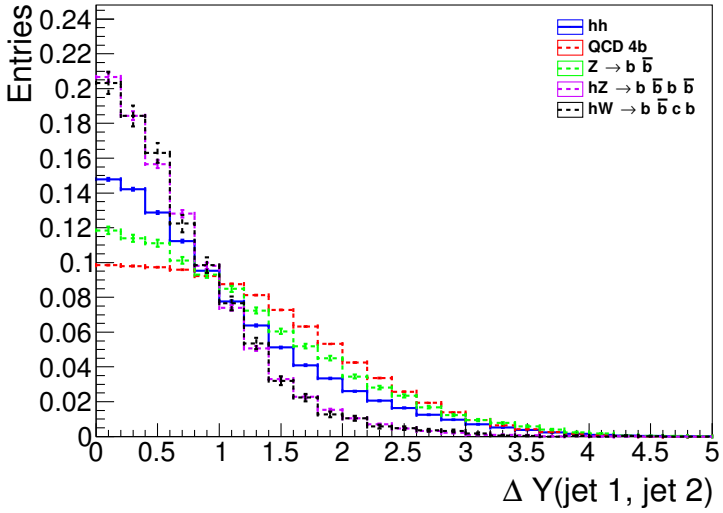

Figure 5: The difference in rapidity between the two leading $R = 1.2$ Cambridge-Aachen jets for the backgrounds and the $\lambda = \lambda_{SM}$ signal.

Higgs boson four-momentum to minimize the background contamination. A mass drop threshold of $\mu = 0.667$ and an asymmetry requirement of $y_{\rm cut} = 0.3$ are used. As soon as a significant mass drop is found in the fat jet, filtering is applied on the jet's constituents, with a filtering radius value, $R_{\rm filt}$, of half the k_t distance between the mass drop elements. The filtering radius is limited to $R_{\rm filt} < 0.3$, following [55], but it is also restricted to $R_{\rm filt} > 0.2$ so as to simulate of the impact of the detector granularity limitation. The three leading filtered jets are taken as a result of this process to reconstruct the Higgs jet. The jet is rejected however, if the two leading filtered jets do not satisfy the b-tagging criteria or have a transverse momentum below 40 GeV. The b-tagging criteria, as in the case of Shower Deconstruction, has 70% efficiency and a 1% false identification rate.

Figure 6 shows the performance of the different 'Higgs boson-tagging' methods we considered in the present article, for the process $pp \to hh \to (b\bar{b})(b\bar{b})$, for $\lambda = \lambda_{SM}$. The performance of the BDRS Higgs boson tagger with a mass cut of ± 20 GeV around the Higgs boson mass is shown, for which the blue star marker (efficiency ~ 0.22) shows the method applied to the leading jet only and the red unfilled star marker (efficiency ~ 0.16) shows the performance for the sub-leading jet. The unfilled black downwards-pointing triangle (efficiency ~ 0.04) shows the performance of simultaneously applying the mass window to both leading and sub-leading jets, while the green filled rhomboid (slightly above) has a further restriction on the rapidity difference between the two jets at $\Delta Y(\text{jet 1, jet 2}) < 2$. The equivalent performance for the Shower Deconstruction Higgs tagger is shown for the same cases in the yellow circle, the black cross, blue square and red up triangle, respectively. Note that the efficiency axis is limited to ~ 0.27, due to the subjets' b-tagging performance, including the 40 GeV threshold for b-tagged jets.

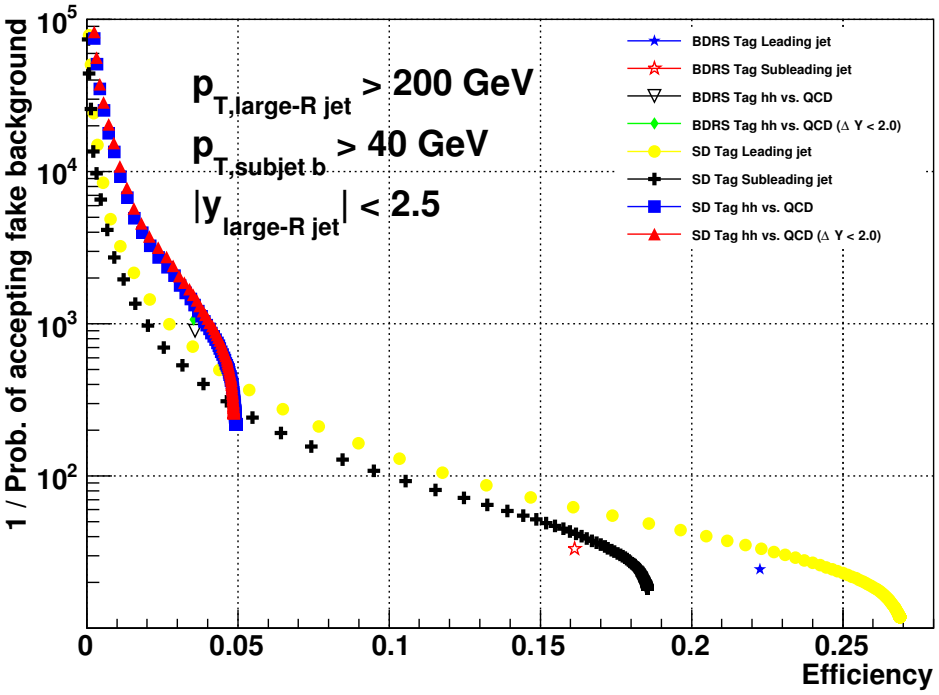

Figure 6: The performance of the different Higgs boson-tagging methods for the process $pp \to hh \to (b\bar{b})(b\bar{b})$, for $\lambda = \lambda_{SM}$. The efficiency includes two b-tags with 70% tagging efficiency and 1% fake rate and $p_{T,\text{b}} \geq 40$ GeV for the single jet tag lines, which is the cause of the limiting effect at $\sim 27\%$ efficiency. The lines showing the performance of tagging two Higgs bosons, include the same effects for both jets.

As we already hinted, the large cut on the jet transverse momentum reduces the effectiveness of the Shower Deconstruction method, which ends up providing an improved, but similar, background rejection as the BDRS method at equal efficiency. Nevertheless, the Shower Deconstruction technique allows one to achieve a high rejection of the backgrounds, by varying the minimum weight requirement. Figure 7 shows the signal-to-background ratio and the significance estimator $s/\sqrt{b}$ for $\lambda = \lambda_{SM}$. The additional rejection given by Shower Deconstruction allows one to have an increased signal-to-background ratio, while maintaining a high value of the significance.

3.3 Constraints

Choosing the Shower Deconstruction setup that yields the maximum value of $s/\sqrt{b}$ from Fig. 7, one can estimate the maximum significance an analysis would obtain with the described cuts. Table 3 shows the cross sections obtained with this selection, either using Shower Deconstruction only or BDRS only for the Higgs jet tag. The first row shows the cross sections after demanding two Cambridge/Aachen jets with $R = 1.2$ and transverse

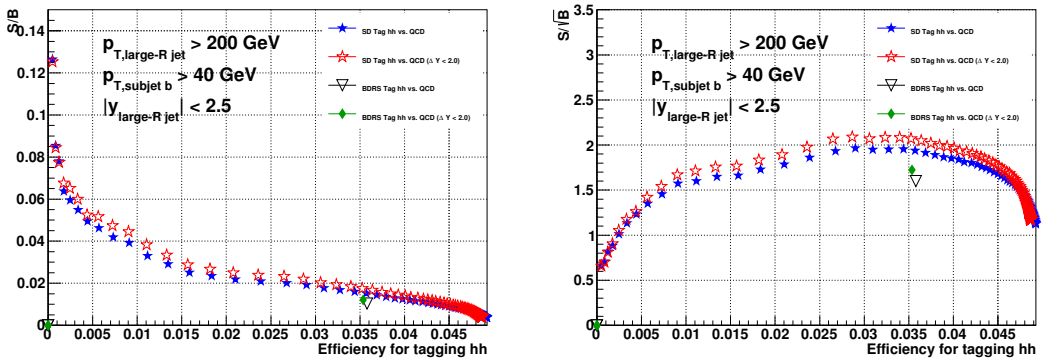

(a) Signal-to-background ratio.

(b) Signal to square root of background ratio.

Figure 7: The signal-to-background ratio and expected significance of the different Higgs boson tagger methods for $\lambda = \lambda_{SM}$.

momentum grater than 200 GeV, with the additional constraint of rapidity $|y| < 2.5$, without the b-tagging criteria.[10]

The following two rows show the effect of applying either Shower Deconstruction or BDRS only to the leading fat jet, including the effect of the two b-tags in its subjets. It also includes the requirement that the two large-R jets satisfy $\Delta Y(\text{jet 1, jet 2}) < 2.0$. The next two rows apply the BDRS or Shower Deconstruction requirements to both jets, showing the final significance obtained of ~ 2.10 using Shower Deconstruction, or ~ 1.74 using only the BDRS technique at 3000 fb^{-1}.

The last two rows in Table 3 show the significance achieved by using a very loose Shower Deconstruction setting with the 26% efficiency point of Fig. 6 and using the BDRS for the sub-leading jet reconstruction. The last row shows the effect of applying a further mass window for the sub-leading jet. This selection configuration can be used to maximise the background in an attempt to implement a data-driven background estimate through a side band analysis, as it will be discussed in Section 3.4.

The analysis procedure can be applied at different values of the Higgs boson self-coupling, and one can take the maximum achievable significance obtained using Shower Deconstruction for each, at 3000 fb^{-1}. The results are shown in Fig. 8. Evidently, for the Standard Model value of the self-coupling, $\lambda/\lambda_{SM} = 1$, it is possible to set a 95% limit using Shower Deconstruction. Due to the reduction in cross section, the significance drops as λ increases. However, the hypothesis of $\lambda = 0$, for example, can be excluded at nearly the 3σ level. The results estimate the significance with the $s/\sqrt{b}$ estimator, taking only statistical uncertainties under consideration.

[10]Note that without the requirement of four b-tags, it cannot be guaranteed that that the shown backgrounds are the dominant ones in this case. Therefore the s/b and $s/\sqrt{b}$ values shown are not realistic and only shown for completeness.

Selection	hh	QCD 4b	hW	Z → bb	hZ	s/b	$s/\sqrt{b}$
Event selection	2.31	6941.860	4.854	266.472	3.787	0.000320	1.48
Leading jet SD	0.514	208.728	0.587	5.360	0.439912	0.00239	1.919
Leading jet BDRS	0.0982	54.223	0.0117	0.741	0.123	0.00178	0.724
Both SD-tags	0.0784	4.226	< 0.00096	0.0294	0.00605	0.0184	2.082
Both BDRS-tags	0.0817	6.671	0.000192	0.0593	0.00946	0.0121	1.723
Loose SD and BDRS rec.	0.621	592.145	0.686	17.228	0.627	0.00101	1.376
Loose SD and BDRS	0.0989	17.080	0.000612	0.129	0.0231	0.00574	1.305

Table 3: Expected cross sections after selection for $\lambda/\lambda_{SM} = 1$. Note that the first row differs from σ_{basic} given in Table 2 due to the additional constraint on the rapidity of the fat jets, $|y| < 2.5$. The significance estimate, $s/\sqrt{b}$, given for an integrated luminosity of 3000 fb^{-1}. The two final rows show the results obtained using Shower Deconstruction on the leading jet and the BDRS for the Higgs reconstruction on the sub-leading one. In the last row a final mass cut on the sub-leading Higgs mass is applied.

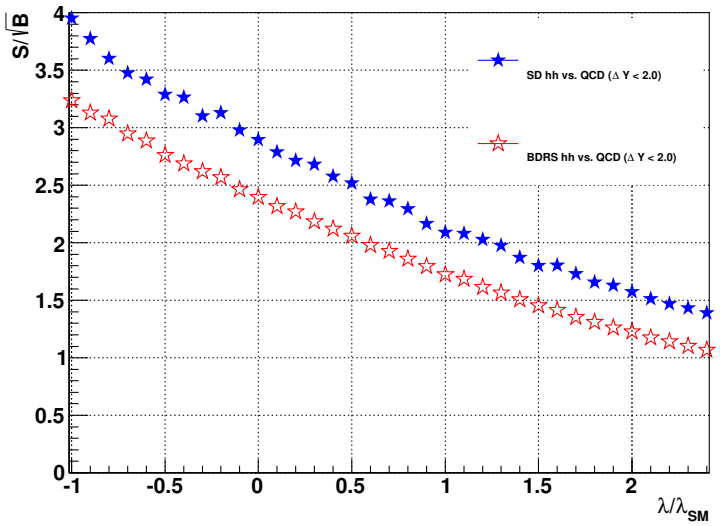

Figure 8: The best expected significance of the different Higgs tagger methods for different values of λ at 3000 fb^{-1} for a 14 TeV LHC.

3.4 Side band analysis

Estimating the background rates and distributions reliably is a very challenging task, as uncertainties originating from the use of Monte Carlo event generators and other theoretical calculations are often too large. An alternative method that can work reasonably well requires an alteration of the selection setup, maximising the background. The background shape and rate can then be modelled in a region where the signal has little or no effect

and subsequently extrapolated to the signal region. With this purpose in mind, the Shower Deconstruction selection for the leading fat jet is loosened to obtain a much lower efficiency of 26% and no mass window is applied using the BDRS tagger for the sub-leading fat jet.

The BDRS-reconstructed mass of the sub-leading jet is shown in Fig. 9, including a model for the leading QCD background using a 5^{th}-order polynomial, shown in the dashed line. The ratio of the remaining backgrounds to the QCD $4b$ fit model is shown in the lower part of the plot with the hh signal and the hZ background weighted by a factor of ten so that they can be compared.

The background estimate can be done by excluding the signal mass window and the Z boson mass region for the QCD $4b$ background model and using the fit to estimate this background's content in the signal region. Other significant backgrounds can be estimated in Monte Carlo simulation and subtracted. These results can be transferred to the signal region with a tighter Shower Deconstruction configuration.

It is interesting to point out that a comparison of the $hh \to (b\bar{b})(b\bar{b})$ signal, which varies with the self-coupling λ, with the $hZ \to (b\bar{b})(b\bar{b})$ background as they both appear in Fig. 9, can be used to estimate the self-coupling as a function of the Higgs-Z coupling.

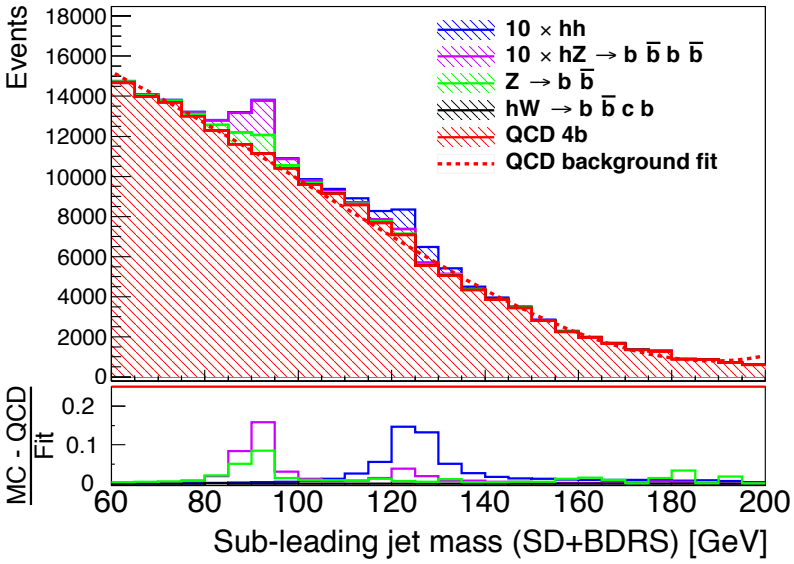

Figure 9: A fit of a side band region using a 5^{th}-order polynomial, performed with looser selection requirements, using Shower Deconstruction for the leading-p_T Higgs boson identification and BDRS for the sub-leading Higgs mass reconstruction. The bottom part of the plot shows the different samples independently normalised by the fit function, to show the relative contribution of each one.

4 Conclusions

Using the BDRS method and Shower Deconstruction on the $(b\bar{b})(b\bar{b})$ final state in Higgs boson pair production, we have demonstrated that it is possible to obtain meaningful con-

straints on the Higgs boson triple self-coupling.

We considered explicitly the main irreducible backgrounds to our signal, including QCD $b\bar{b}b\bar{b}$, electroweak/QCD $Zb\bar{b}$ with $Z \to b\bar{b}$ and electroweak $hZ \to (b\bar{b})(b\bar{b})$, as well as the reducible hW background containing charm-quark jets mis-tagged as b jets. Including reducible backgrounds will not significantly alter our conclusions after requiring 4 b-tags. Moreover, we have demonstrated that a side-band analysis using Shower Deconstruction for the leading Higgs boson jet and BDRS for the sub-leading Higgs mass reconstruction can be a viable option in measuring the Higgs boson self-coupling.

We conclude that at an LHC running at 14 TeV, with 3000 fb^{-1} of integrated luminosity, the self-coupling can be constrained to $\lambda \lesssim 1.2 \times \lambda_{SM}$ at 95% confidence level based on statistical considerations alone, since no theoretical uncertainties have been included. Nevertheless, using the side-band analysis proposed one could estimate the background to good accuracy by extrapolating the background content from real data in the side band into the signal region.

Further improvements are possible: refined trigger and b-tagging strategies can help to retain more signal and allow novel reconstruction techniques to achieve a better performance. These conclusions motivate in-depth examination of the $(b\bar{b})(b\bar{b})$ final state in Higgs boson by the LHC experimental collaborations.

Acknowledgments

AP would like to thank Paolo Torrielli for useful discussion and acknowledges supported in part by the Swiss National Science Foundation (SNF) under contract 200020-149517 and by the European Commission through the "LHCPhenoNet" Initial Training Network PITN-GA-2010-264564 and MCnetITN FP7 Marie Curie Initial Training Network PITN-GA-2012-315877.

References

[1] **ATLAS** Collaboration, G. Aad et al., *Observation of a new particle in the search for the Standard Model Higgs boson with the ATLAS detector at the LHC*, *Phys.Lett.* **B716** (2012) 1–29, [arXiv:1207.7214].

[2] **CMS** Collaboration, S. Chatrchyan et al., *Observation of a new boson at a mass of 125 GeV with the CMS experiment at the LHC*, *Phys.Lett.* **B716** (2012), no. CMS-HIG-12-028, CERN-PH-EP-2012-220 30–61, [arXiv:1207.7235].

[3] **CMS** Collaboration, *Combination of standard model Higgs boson searches and measurements of the properties of the new boson with a mass near 125 GeV*, Tech. Rep. CMS-PAS-HIG-12-045, CERN, 2012.

[4] **ATLAS** Collaboration, *Coupling properties of the new Higgs-like boson observed with the ATLAS detector at the LHC*, Tech. Rep. ATLAS-CONF-2012-127, ATLAS-COM-CONF-2012-161, CERN, 2012.

[5] **ATLAS** Collaboration, *An update of combined measurements of the new Higgs-like boson with high mass resolution channels*, Tech. Rep. ATLAS-CONF-2012-170, CERN, Geneva, Dec, 2012.

[6] S. Kanemura, S. Kiyoura, Y. Okada, E. Senaha, and C. Yuan, *New physics effect on the Higgs selfcoupling*, *Phys.Lett.* **B558** (2003) 157–164, [hep-ph/0211308].

[7] J. Grigo, J. Hoff, K. Melnikov, and M. Steinhauser, *On the Higgs boson pair production at the LHC*, *Nucl.Phys.* **B875** (2013) 1–17, [arXiv:1305.7340].

[8] T. Plehn and M. Rauch, *The quartic higgs coupling at hadron colliders*, *Phys.Rev.* **D72** (2005) 053008, [hep-ph/0507321].

[9] T. Binoth, S. Karg, N. Kauer, and R. Ruckl, *Multi-Higgs boson production in the Standard Model and beyond*, *Phys.Rev.* **D74** (2006) 113008, [hep-ph/0608057].

[10] D. Miller and S. Moretti, *Can the trilinear Higgs selfcoupling be measured at future linear colliders?*, *Eur.Phys.J.* **C13** (2000) 459–470, [hep-ph/9906395].

[11] E. N. Glover and J. van der Bij, *Higgs boson pair production via gluon fusion*, *Nucl.Phys.* **B309** (1988) 282.

[12] S. Dawson, S. Dittmaier, and M. Spira, *Neutral Higgs boson pair production at hadron colliders: QCD corrections*, *Phys.Rev.* **D58** (1998) 115012, [hep-ph/9805244].

[13] A. Djouadi, W. Kilian, M. Muhlleitner, and P. Zerwas, *Production of neutral Higgs boson pairs at LHC*, *Eur.Phys.J.* **C10** (1999) 45–49, [hep-ph/9904287].

[14] T. Plehn, M. Spira, and P. Zerwas, *Pair production of neutral Higgs particles in gluon-gluon collisions*, *Nucl.Phys.* **B479** (1996) 46–64, [hep-ph/9603205].

[15] U. Baur, T. Plehn, and D. L. Rainwater, *Determining the Higgs boson selfcoupling at hadron colliders*, *Phys.Rev.* **D67** (2003) 033003, [hep-ph/0211224].

[16] U. Baur, T. Plehn, and D. L. Rainwater, *Probing the Higgs selfcoupling at hadron colliders using rare decays*, *Phys.Rev.* **D69** (2004) 053004, [hep-ph/0310056].

[17] M. J. Dolan, C. Englert, and M. Spannowsky, *Higgs self-coupling measurements at the LHC*, *JHEP* **1210** (2012) 112, [arXiv:1206.5001].

[18] J. Baglio, A. Djouadi, R. Grober, M. Muhlleitner, J. Quevillon, et al., *The measurement of the Higgs self-coupling at the LHC: theoretical status*, arXiv:1212.5581.

[19] A. J. Barr, M. J. Dolan, C. Englert, and M. Spannowsky, *Di-Higgs final states augMT2ed – selecting hh events at the high luminosity LHC*, arXiv:1309.6318.

[20] M. J. Dolan, C. Englert, N. Greiner, and M. Spannowsky, *Further on up the road: hhjj production at the LHC*, arXiv:1310.1084.

[21] A. Papaefstathiou, L. L. Yang, and J. Zurita, *Higgs boson pair production at the LHC in the $b\bar{b}W^+W^-$ channel*, arXiv:1209.1489.

[22] F. Goertz, A. Papaefstathiou, L. L. Yang, and J. Zurita, *Higgs Boson self-coupling measurements using ratios of cross sections*, arXiv:1301.3492.

[23] F. Goertz, A. Papaefstathiou, L. L. Yang, and J. Zurita, *Measuring the Higgs boson self-coupling at the LHC using ratios of cross sections*, arXiv:1309.3805.

[24] D. de Florian and J. Mazzitelli, *Higgs pair production at NNLO*, arXiv:1309.6594.

[25] D. de Florian and J. Mazzitelli, *Two-loop virtual corrections to Higgs pair production*, *Phys.Lett.* **B724** (2013) 306–309, [arXiv:1305.5206].

[26] J. Cao, Z. Heng, L. Shang, P. Wan, and J. M. Yang, *Pair Production of a 125 GeV Higgs Boson in MSSM and NMSSM at the LHC*, *JHEP* **1304** (2013) 134, [arXiv:1301.6437].

[27] R. S. Gupta, H. Rzehak, and J. D. Wells, *How well do we need to measure the Higgs boson mass and self-coupling?*, *Phys.Rev.* **D88** (2013) 055024, [arXiv:1305.6397].

[28] D. T. Nhung, M. Muhlleitner, J. Streicher, and K. Walz, *Higher Order Corrections to the Trilinear Higgs Self-Couplings in the Real NMSSM*, arXiv:1306.3926.

[29] U. Ellwanger, *Higgs pair production in the NMSSM at the LHC*, *JHEP* **1308** (2013) 077, [arXiv:1306.5541].

[30] J. M. No and M. Ramsey-Musolf, *Probing the Higgs Portal at the LHC Through Resonant di-Higgs Production*, arXiv:1310.6035.

[31] M. McCullough, *A New Indirect Probe of the Higgs Self-Coupling*, arXiv:1312.3322.

[32] P. Maierhöefer and A. Papaefstathiou, *Higgs Boson pair production merged to one jet*, arXiv:1401.0007.

[33] W. Hollik and S. Penaranda, *Yukawa coupling quantum corrections to the selfcouplings of the lightest MSSM Higgs boson*, *Eur.Phys.J.* **C23** (2002) 163–172, [hep-ph/0108245].

[34] M. Dubinin and A. Semenov, *Triple and quartic interactions of Higgs bosons in the general two Higgs doublet model*, hep-ph/9812246.

[35] J. Tian and K. Fujii, *Measurement of Higgs couplings and self-coupling at the ILC*, arXiv:1311.6528.

[36] S. Dawson, A. Gritsan, H. Logan, J. Qian, C. Tully, et al., *Working Group Report: Higgs Boson*, arXiv:1310.8361.

[37] R. Lafaye, D. Miller, M. Muhlleitner, and S. Moretti, *Double Higgs production at TeV colliders in the minimal supersymmetric standard model*, hep-ph/0002238.

[38] P. Osland and P. Pandita, *Multiple Higgs production and measurement of Higgs trilinear couplings in the MSSM*, hep-ph/9911295.

[39] P. Osland, *Higgs boson production in e+ e- and e- e- collisions*, *Acta Phys.Polon.* **B30** (1999) 1967–1984, [hep-ph/9903301].

[40] M. Brucherseifer, R. Gavin, and M. Spira, *MSSM Higgs Self-Couplings: Two-Loop $\mathcal{O}(\alpha_t\alpha_s)$ Corrections*, arXiv:1309.3140.

[41] W. Yao, *Studies of measuring Higgs self-coupling with $HH \to b\bar{b}\gamma\gamma$ at the future hadron colliders*, arXiv:1308.6302.

[42] R. Frederix, S. Frixione, V. Hirschi, F. Maltoni, O. Mattelaer, et al., *Higgs pair production at the LHC with NLO and parton-shower effects*, *Phys.Lett.* **B732** (2014) 142–149, [arXiv:1401.7340].

[43] M. H. Seymour, *Searches for new particles using cone and cluster jet algorithms: A Comparative study*, *Z.Phys.* **C62** (1994) 127–138.

[44] U. Baur, T. Plehn, and D. L. Rainwater, *Examining the Higgs boson potential at lepton and hadron colliders: A Comparative analysis*, *Phys.Rev.* **D68** (2003) 033001, [hep-ph/0304015].

[45] M. J. Dolan, C. Englert, and M. Spannowsky, *New Physics in LHC Higgs boson pair production*, arXiv:1210.8166.

[46] M. Gouzevitch, A. Oliveira, J. Rojo, R. Rosenfeld, G. P. Salam, et al., *Scale-invariant resonance tagging in multijet events and new physics in Higgs pair production*, *JHEP* **1307** (2013) 148, [arXiv:1303.6636].

[47] A. Efrati and Y. Nir, *What if $\lambda_{hhh} \neq 3m_h^2/v$*, arXiv:1401.0935.

[48] *A search for resonant Higgs-pair production in the $b\bar{b}b\bar{b}$ final state in pp collisions at $\sqrt{s} = 8$ TeV*, Tech. Rep. ATLAS-CONF-2014-005, CERN, Geneva, Mar, 2014.

[49] B. Cooper, N. Konstantinidis, L. Lambourne, and D. Wardrope, *Boosted $hh \to b\bar{b}b\bar{b}$: a new topology in searches for TeV-scale resonances at the LHC*, *Phys.Rev.* **D88** (2013) 114005, [arXiv:1307.0407].

[50] C. Han, X. Ji, L. Wu, P. Wu, and J. M. Yang, *Higgs pair production with SUSY QCD correction: revisited under current experimental constraints*, *JHEP* **1404** (2014) 003, [arXiv:1307.3790].

[51] D. Y. Shao, C. S. Li, H. T. Li, and J. Wang, *Threshold resummation effects in Higgs boson pair production at the LHC*, arXiv:1301.1245.

[52] Y. Philippov, *Yukawa radiative corrections to the trilinear self-couplings of neutral CP-even Higgs bosons and decay width Gamma ($H \to hh$) in the MSSM*, *Phys.Atom.Nucl.* **70** (2007) 1288–1293, [hep-ph/0611260].

[53] M. Dolgopolov and Y. Philippov, *The Trilinear neutral Higgs selfcouplings in the MSSM: Complete one loop analysis*, hep-ph/0310018.

[54] F. Boudjema and A. Semenov, *Measurements of the SUSY Higgs selfcouplings and the reconstruction of the Higgs potential*, *Phys.Rev.* **D66** (2002) 095007, [hep-ph/0201219].

[55] J. M. Butterworth, A. R. Davison, M. Rubin, and G. P. Salam, *Jet substructure as a new Higgs search channel at the LHC*, *Phys.Rev.Lett.* **100** (2008) 242001, [arXiv:0802.2470].

[56] D. E. Soper and M. Spannowsky, *Finding physics signals with shower deconstruction*, *Phys.Rev.* **D84** (2011) 074002, [arXiv:1102.3480].

[57] D. E. Soper and M. Spannowsky, *Finding top quarks with shower deconstruction*, *Phys.Rev.* **D87** (2013), no. 5 054012, [arXiv:1211.3140].

[58] D. E. Soper and M. Spannowsky, *Finding physics signals with event deconstruction*, arXiv:1402.1189.

[59] R. S. Bartoldus, C. M. C. Bee, D. C. Francis, N. R. Gee, S. L. R. George, R. M. S. Hauser, R. R. Middleton, T. C. Pauly, O. K. Sasaki, D. O. Strom, R. R. I. Vari, and S. R. I. Veneziano, *Technical Design Report for the Phase-I Upgrade of the ATLAS TDAQ System*, Tech. Rep. CERN-LHCC-2013-018. ATLAS-TDR-023, CERN, Geneva, Sep, 2013. Final version presented to December 2013 LHCC.

[60] T. A. collaboration, *Search for the Standard Model Higgs boson produced in association with top quarks and decaying to $b\bar{b}$ in pp collisions at $\sqrt{s} = 8$ TeV with the ATLAS detector at the LHC*, .

[61] J. Thaler and K. Van Tilburg, *Identifying Boosted Objects with N-subjettiness*, *JHEP* **1103** (2011) 015, [arXiv:1011.2268].

[62] D. E. Soper and M. Spannowsky, *Combining subjet algorithms to enhance ZH detection at the LHC*, *JHEP* **1008** (2010) 029, [arXiv:1005.0417].

[63] M. Backovic, J. Juknevich, and G. Perez, *Boosting the Standard Model Higgs Signal with the Template Overlap Method*, *JHEP* **1307** (2013) 114, [arXiv:1212.2977].

[64] L. G. Almeida, O. Erdogan, J. Juknevich, S. J. Lee, G. Perez, et al., *Three-particle templates for a boosted Higgs boson*, *Phys.Rev.* **D85** (2012) 114046, [arXiv:1112.1957].

[65] S. D. Ellis, A. Hornig, T. S. Roy, D. Krohn, and M. D. Schwartz, *Qjets: A Non-Deterministic Approach to Tree-Based Jet Substructure*, *Phys.Rev.Lett.* **108** (2012) 182003, [arXiv:1201.1914].

[66] M. Bahr, S. Gieseke, M. Gigg, D. Grellscheid, K. Hamilton, et al., *Herwig++ Physics and Manual*, *Eur.Phys.J.* **C58** (2008) 639–707, [arXiv:0803.0883].

[67] K. Arnold, L. d'Errico, S. Gieseke, D. Grellscheid, K. Hamilton, et al., *Herwig++ 2.6 Release Note*, arXiv:1205.4902.

[68] J. Bellm, S. Gieseke, D. Grellscheid, A. Papaefstathiou, S. Platzer, et al., *Herwig++ 2.7 Release Note*, arXiv:1310.6877.

[69] "hpair program." http://people.web.psi.ch/spira/hpair/.

[70] M. L. Mangano, M. Moretti, F. Piccinini, R. Pittau, and A. D. Polosa, *ALPGEN, a generator for hard multiparton processes in hadronic collisions*, *JHEP* **0307** (2003) 001, [hep-ph/0206293].

[71] S. Frixione, F. Stoeckli, P. Torrielli, and B. R. Webber, *NLO QCD corrections in Herwig++ with MC@NLO*, *JHEP* **1101** (2011) 053, [arXiv:1010.0568].

[72] J. Alwall, M. Herquet, F. Maltoni, O. Mattelaer, and T. Stelzer, *MadGraph 5 : Going Beyond*, *JHEP* **1106** (2011) 128, [arXiv:1106.0522].

[73] J. Alwall, R. Frederix, S. Frixione, V. Hirschi, F. Maltoni, et al., *The automated computation of tree-level and next-to-leading order differential cross sections, and their matching to parton shower simulations*, arXiv:1405.0301.

[74] T. Binoth, N. Greiner, A. Guffanti, J. Reuter, J.-P. Guillet, et al., *Next-to-leading order QCD corrections to pp $\to$ b anti-b b anti-b + X at the LHC: the quark induced case*, *Phys.Lett.* **B685** (2010) 293–296, [arXiv:0910.4379].

[75] N. Greiner, A. Guffanti, T. Reiter, and J. Reuter, *NLO QCD corrections to the production of two bottom-antibottom pairs at the LHC*, *Phys.Rev.Lett.* **107** (2011) 102002, [arXiv:1105.3624].